Electronic Supplementary Material (ESI) for Green Chemistry.
This journal is © The Royal Society of Chemistry 2019

Supplementary Information

Biomass-Derived N-Doped Porous Carbon: An Efficient Metal-free Catalyst for Methylation of Amines with CO_2

Feiying Tang,[a] Liqiang Wang,*[a,b] and You-Nian Liu*[a,b]

[a] College of Chemistry and Chemical Engineering, Central South University, Changsha, Hunan 410083, P.R. China.

[b] State Key Laboratory of Powder Metallurgy, Central South University, Changsha, Hunan 410083, P.R. China.

*Corresponding Authors: E-mail addresses: liqiangwang@csu.edu.cn (L. Wang) and liuyounian@csu.edu.cn (Y.-N. Liu). Phone/Fax: +86-731-8887-9616.

Contents

b) Pore size distribution for $NPC_{(1/2)}$, $NPC_{(1/3)}$, $NPC_{(1/5)}$ and $NPC_{(1/7)}$.

Fig. S9. a) CO_2 adsorption (273 K and 298 K) and b) heat of adsorption of $NPC_{(1/2)}$, $NPC_{(1/3)}$, $NPC_{(1/5)}$ and $NPC_{(1/7)}$.

Fig. S10. The HPLC spectra of N-methylaniline, N, N-dimethylaniline, N-methylformanilide and the mixture under reaction.

Fig. S11. The kinetic data on the methylation reaction over $NPC_{(1/5)}$.

Fig. S12. XPS analysis on $NPC_{(1/5)}$ before and after the reaction.

Fig. S13. Optimized initial state (I), transition state (TS) and final state (F) structures involved in step i. Some selected distances are given in Å.

Fig. S14. Optimized initial state (I), transition state (TS) and final state (F) structures involved of step ii. Some selected distances are given in Å.

Fig. S15. Optimized initial state (I), transition state (TS) and final state (F) structures involved of step iii. Some selected distances are given in Å.

Fig. S16. Optimized initial state (I), transition state (TS) and final state (F) structures involved of step iv. Some selected distances are given in Å.

4. Tables

Table S1. Summary of N 1s XPS results for NPC samples.

Table S2. Summary of surface areas and pore volumes for all NPC samples.

Table S3. Catalytic performance of $NPC_{(1/5)}$ in different solvents.

Table S4. The Methylation reaction of N-methylaniline with CO_2 over our proposed NPC catalysts and recently documented homogenous catalyst.

Table S5. Summary of N 1s XPS results for NPC(1/5) before and after reaction.

1. Experimental

Materials. All chemicals in this work were purchased from Titan Technology Co. Ltd. (Shanghai, China). All chemicals were of analytical grade without further purification.

Preparation of Catalysts. Nitrogen-doped porous carbon (NPC) was synthesized as follows: first, the tannic acid and urea were dissolved into water (the mass ratios of tannic acid to urea were kept at 1:2, 1:3, 1:5 and 1:7), followed by drying at 75 ºC. The obtained solid was moved into a tubular furnace for pyrolysis under N_2 flow (80 mL min^{-1}). The sample was firstly heated to 600 ºC at a heating rate of 2 ºC min^{-1} and maintained for 1 h, then heated to 900 ºC at 2 ºC min^{-1} and maintained for 1 h, then cool down to the room temperature. The obtained NPC samples were named as $NPC_{(1/2)}$, $NPC_{(1/3)}$, $NPC_{(1/5)}$ and $NPC_{(1/7)}$ correspondingly.

Characterization of Catalysts. X-ray diffraction (XRD) data were measured on a Bruke D8 diffractometer (Bruke, Germany) with Cu Ka (k = 1.5418 Å) radiation (50 kV, 30 mA). Scanning electron microscopy (SEM) images were obtained with an S-4800 (Hitachi, Japan). Transmission electron microscopy (TEM) images were taken on an instrument Tecnai G2-20 (FEI, USA). X-ray photoelectron spectra (XPS) was collected on 250XI spectrometer (Shimadzu, Japan) equipped with an Al Ka (1486.6 eV) irradiation source. Nitrogen (N_2) adsorption-desorption isotherms were obtained by static N_2 physisorption at 77 k with a Quantachrome Autosorb iQ analyser (Quantachrome, USA). The surface area was measured by using the multipoint Brunauer-Emmett-Teller (BET) method. The pore volume and pore size were

evaluated from desorption branches of the isotherms with the Barrett-Joyner-Halenda (BJH) method. Raman spectra were measured on an inVia confocal Raman microscope (Renishaw, UK) equipped with a He-Ne laser (l = 532 nm). CO_2 TPD were taken on AutoChem1 II 2920 as follows, firstly heat to 650 ^oC by 10 ^oC min^{-1}, then the sample was activated for 40 min at 650 ^oC. The samples were subsequently exposed to pulses of CO_2 until saturation and then purged with helium (He) flow at 100 ^oC for 1 h. The temperature of the samples was increased to 600 ^oC at a ramping rate of 10 ^oC min^{-1}, and the desorbed CO_2 was detected and collected the data.

Measurement of catalytic performance. The methylation of CO_2 was conducted in presence of 0.25 mmol substrate, 0.5 mmol phenylsilane, 3 ml solvent, 15 mg catalyst and 0.1 MPa CO_2 (a balloon filled with CO_2) at the temperature of 75 ^oC for 20 h under vigorous stirring. After the solvents cooling down to room temperature, the conversion and selectivity of products were detected by using HPLC (LC-20AD, Shimadzu, Japan).

The catalyst was recycled by centrifugation, then washed by EtOH for several times and dried at 80 ^oC. The recycled catalyst was reused under the same reaction conditions for the recyclability tests.

Computational method and model. All calculations were performed by using the functional Dmol3 in material studio. The TS (transition state) Search was performed by using the generalized gradient approximation (GGA) with the BP functional in Dmol3 method. The reaction barrier $E_{(b)}$ was calculated by

$$E_{(b)} = E_{(TS)} - E_{(IS)}$$

Where $E_{(IS)}$, $E_{(FS)}$, and $E_{(TS)}$ represent the energy of the initial state (IS), final state (FS), and transition state (TS), respectively.

2. Schemes

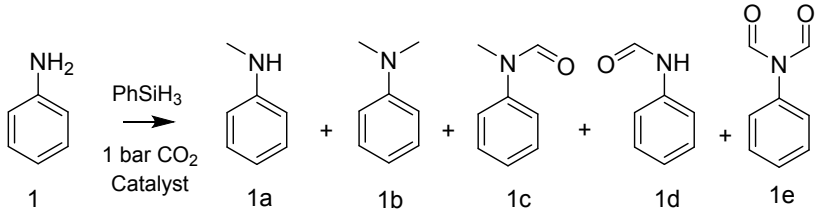

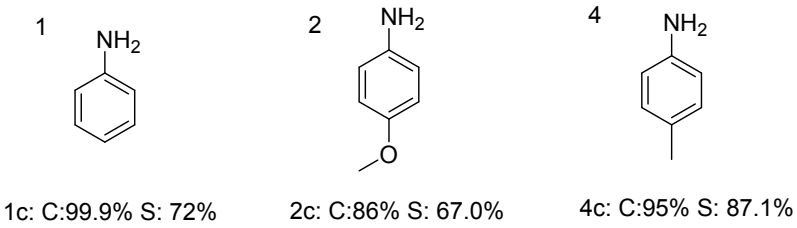

1c: C:99.9% S: 72% 2c: C:86% S: 67.0% 4c: C:95% S: 87.1%

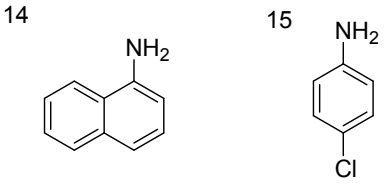

14c: C:98% S: 72.9% 15c: C:97% S: 80.6%

Scheme S1. Catalytic reaction of primary amine with CO_2 by using $NPC_{(1/5)}$.

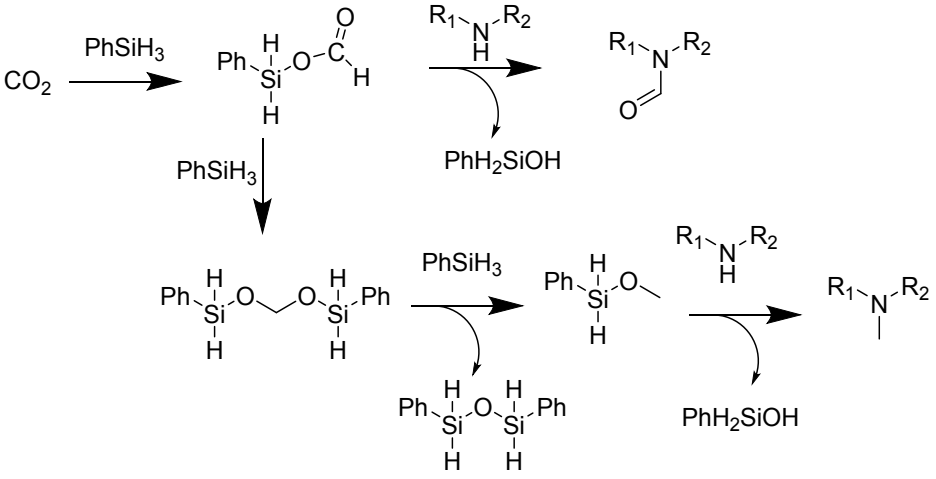

Scheme S2. Proposed reaction pathway for CO_2 conversion.

3. Figures

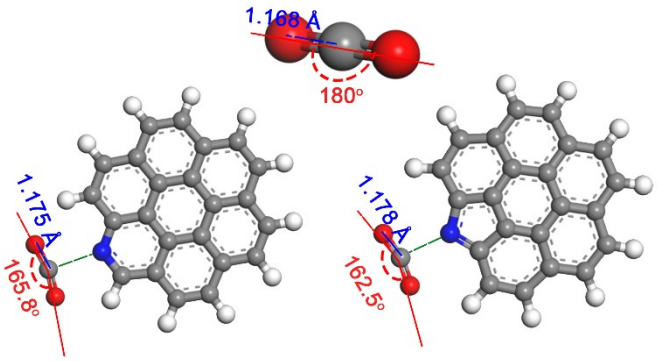

Fig. S1. The interaction of CO_2 with pyridinic N and pyrrolic N, respectively.

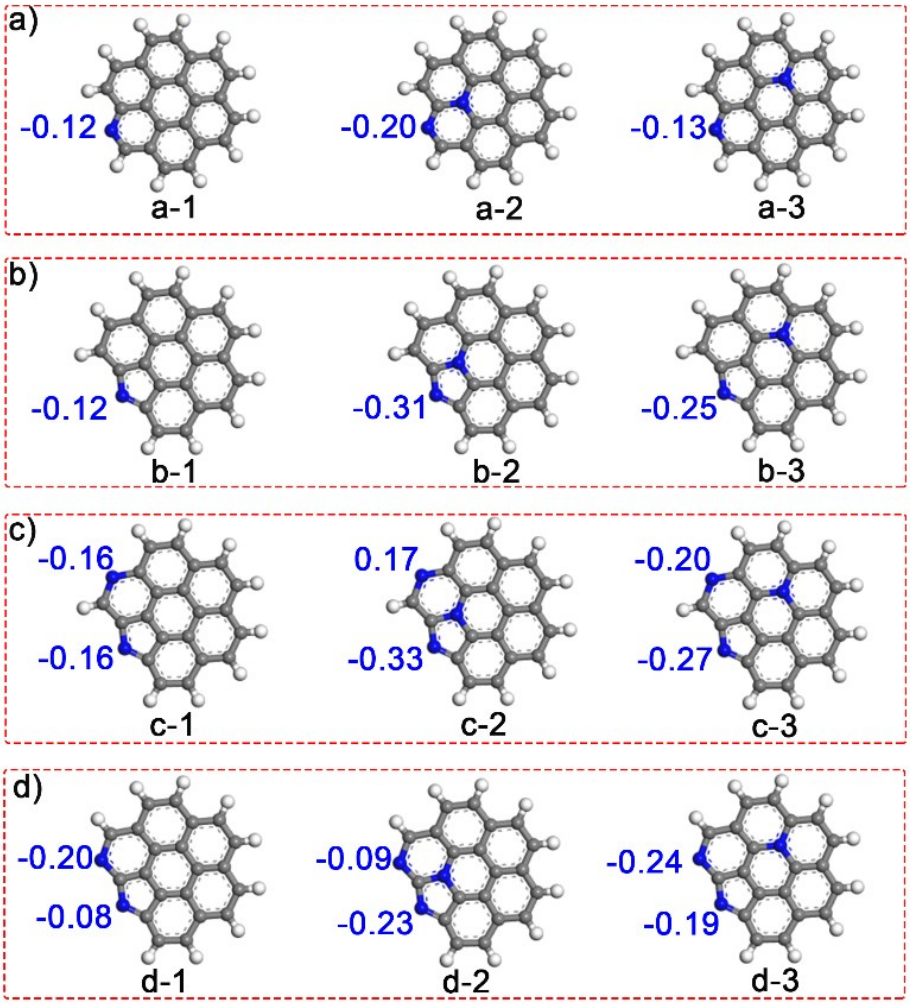

Fig. S2. Hirshfeld charge population analysis results of N-species on various simulated NPC models.

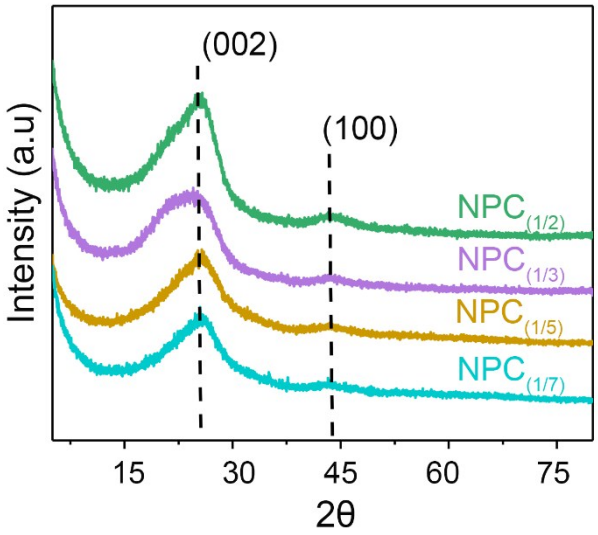

Fig. S3. XRD patterns of $NPC_{(1/2)}$, $NPC_{(1/3)}$, $NPC_{(1/5)}$ and $NPC_{(1/7)}$.

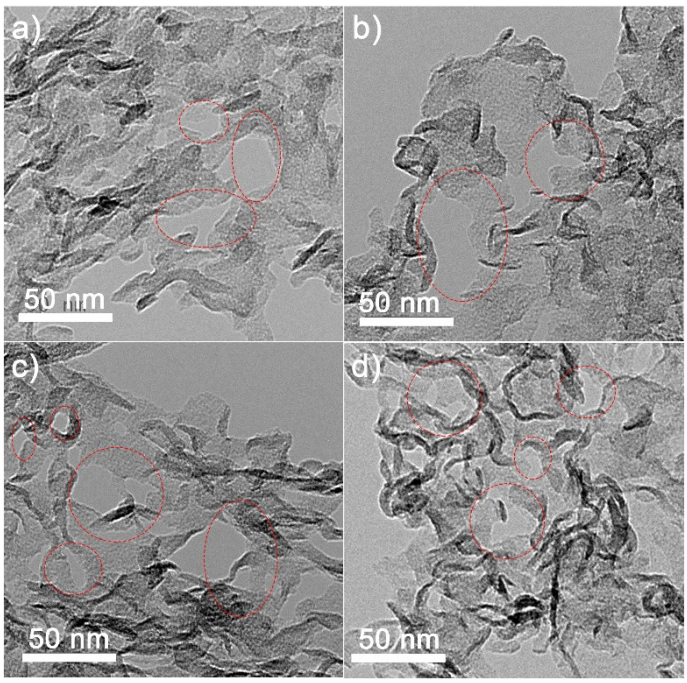

Fig. S4. TEM images of a) $NPC_{(1/2)}$, b) $NPC_{(1/3)}$, c) $NPC_{(1/5)}$ and d) $NPC_{(1/7)}$.

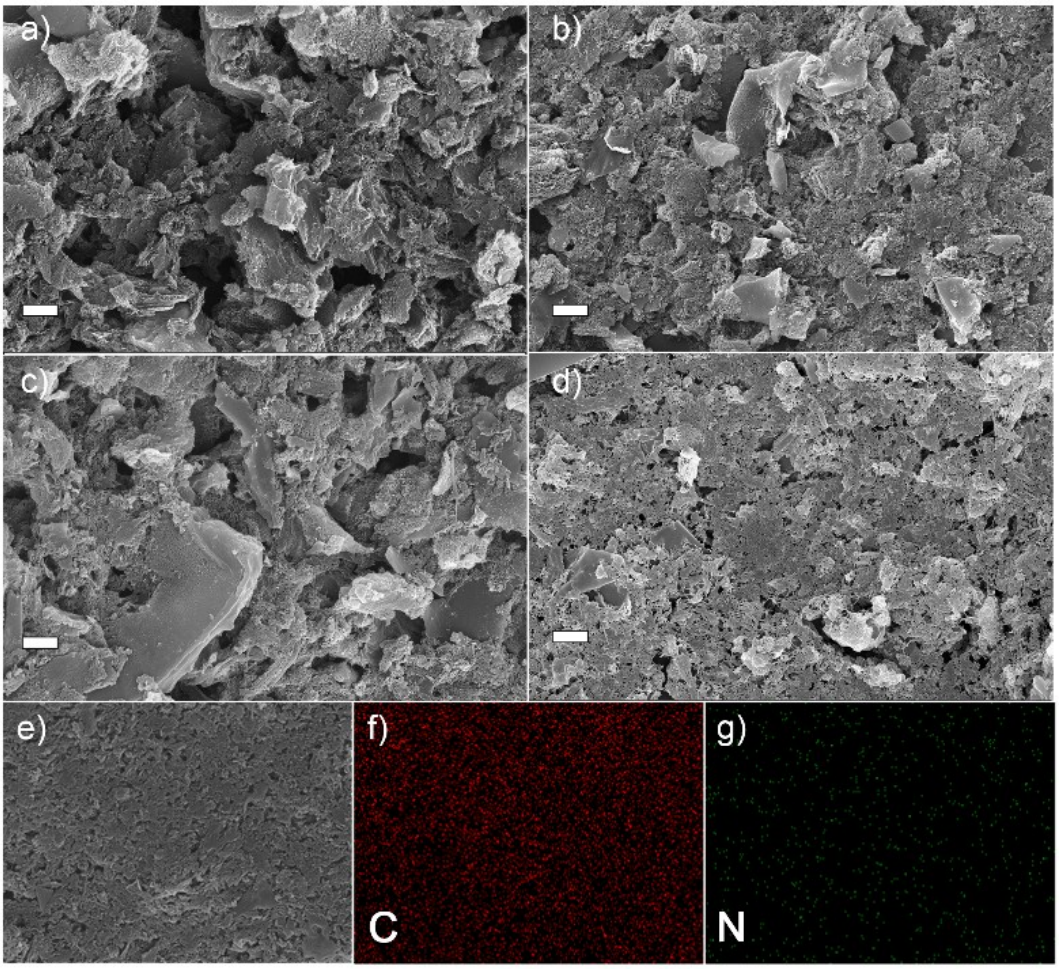

Fig. S5. SEM images of a) $NPC_{(1/2)}$, b) $NPC_{(1/3)}$, c) $NPC_{(1/5)}$ and d) $NPC_{(1/7)}$. e) SEM image of $NPC_{(1/5)}$ and the corresponding EDX mapping of) C and g) N elements. Scale bar: 200 nm.

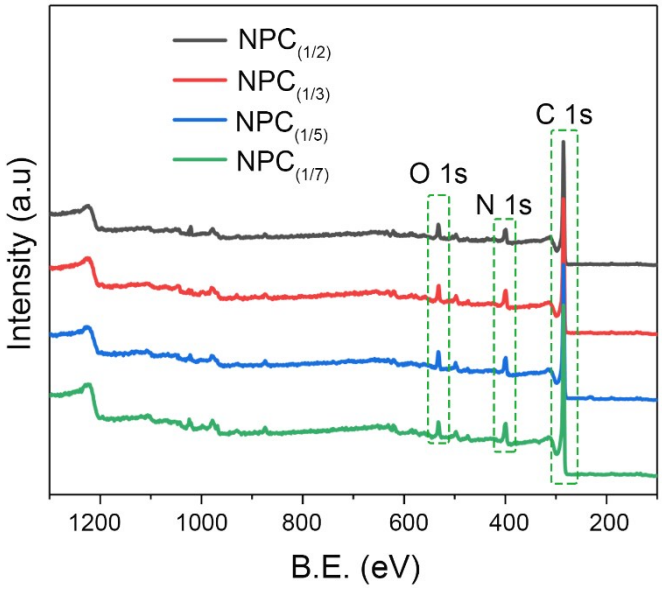

Fig. S6. XPS survey spectra of $NPC_{(1/2)}$, $NPC_{(1/3)}$, $NPC_{(1/5)}$ and $NPC_{(1/7)}$.

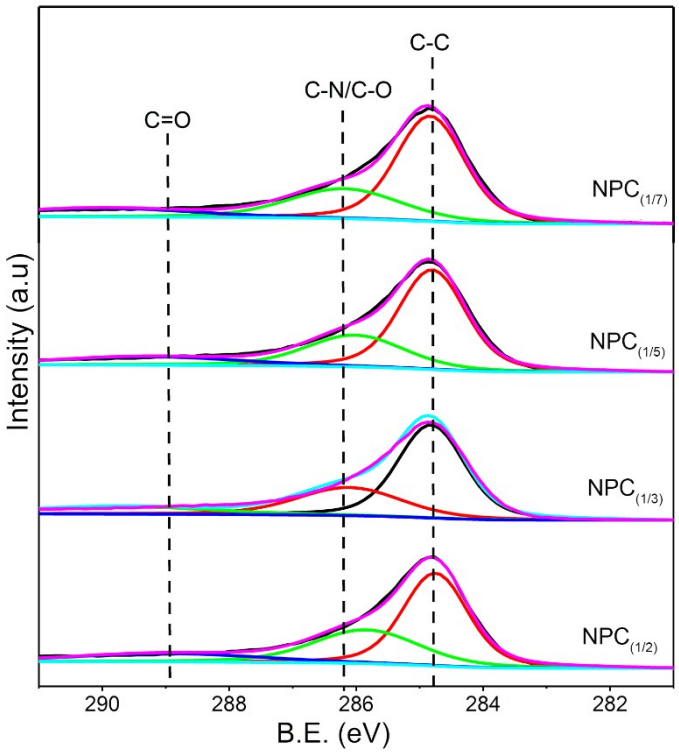

Fig. S7. C 1s XPS spectra of $NPC_{(1/2)}$, $NPC_{(1/3)}$, $NPC_{(1/5)}$ and $NPC_{(1/7)}$.

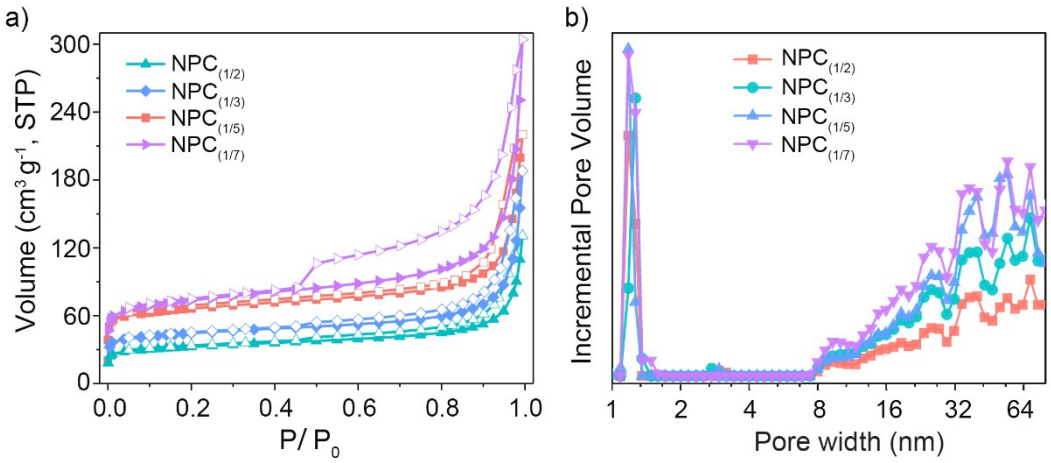

Fig. S8. a) N_2 Adsorption (filled symbols)/desorption (empty symbols) isotherms and b) Pore size distribution for $NPC_{(1/2)}$, $NPC_{(1/3)}$, $NPC_{(1/5)}$ and $NPC_{(1/7)}$.

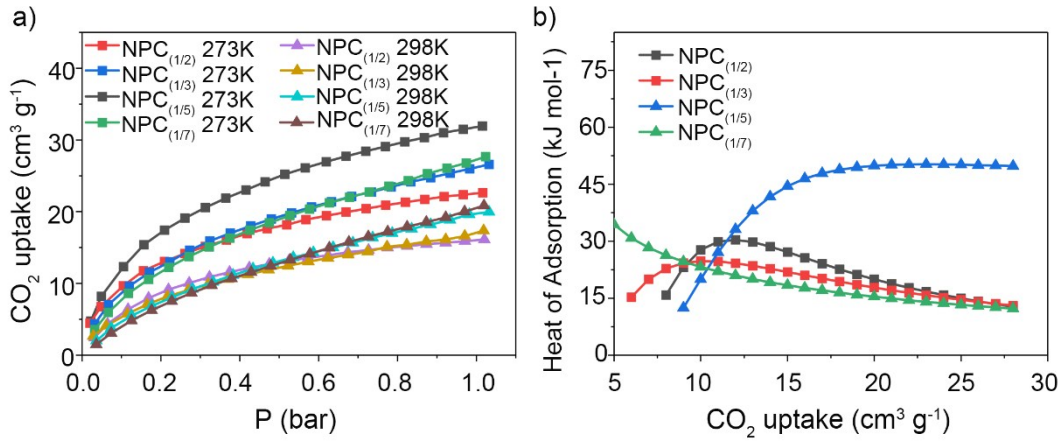

Fig. S9. a) CO_2 adsorption (273 K and 298 K) and b) heat of adsorption of $NPC_{(1/2)}$, $NPC_{(1/3)}$, $NPC_{(1/5)}$ and $NPC_{(1/7)}$.

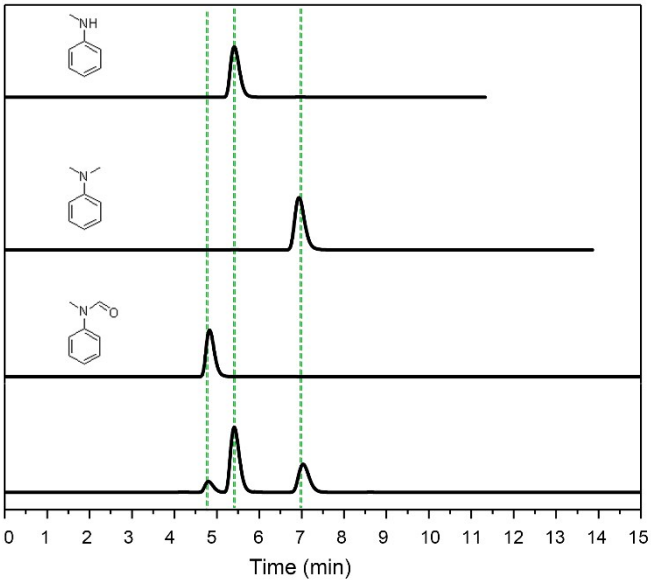

Fig. S10. The HPLC spectra of N-methylaniline, N, N-dimethylaniline, N-methylformanilide and the mixture under reaction. The reaction mixture was analyzed via HPLC. The mobile phase is CH_3OH/H_2O (0.18/0.62, v/v). The retention time of N-methylaniline, N, N-dimethylaniline and N-methylformanilide are 5.42, 6.93 and 4.81 min, respectively.

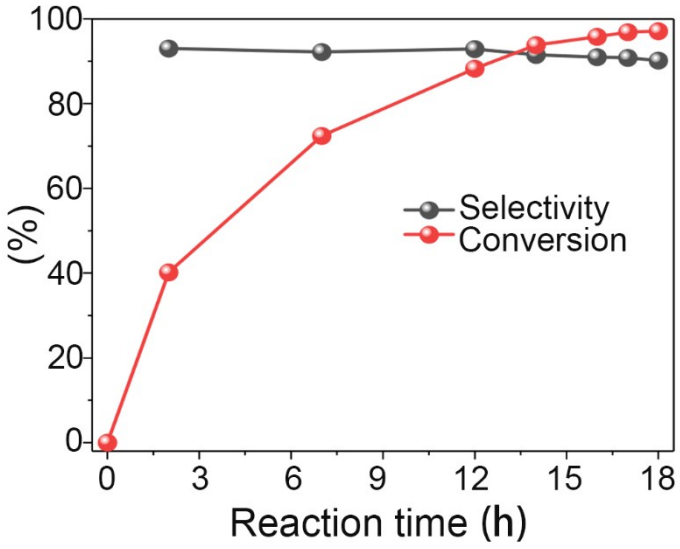

Fig. S11. The kinetic data on the methylation reaction over $NPC_{(1/5)}$.

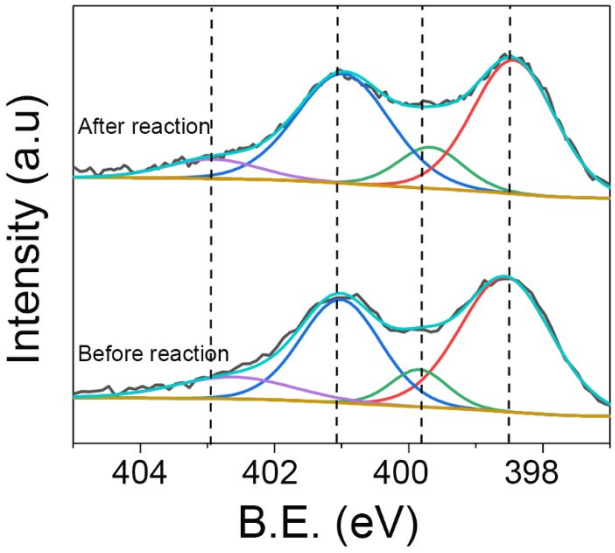

Fig. S12. XPS analysis on $NPC_{(1/5)}$ before and after the reaction.

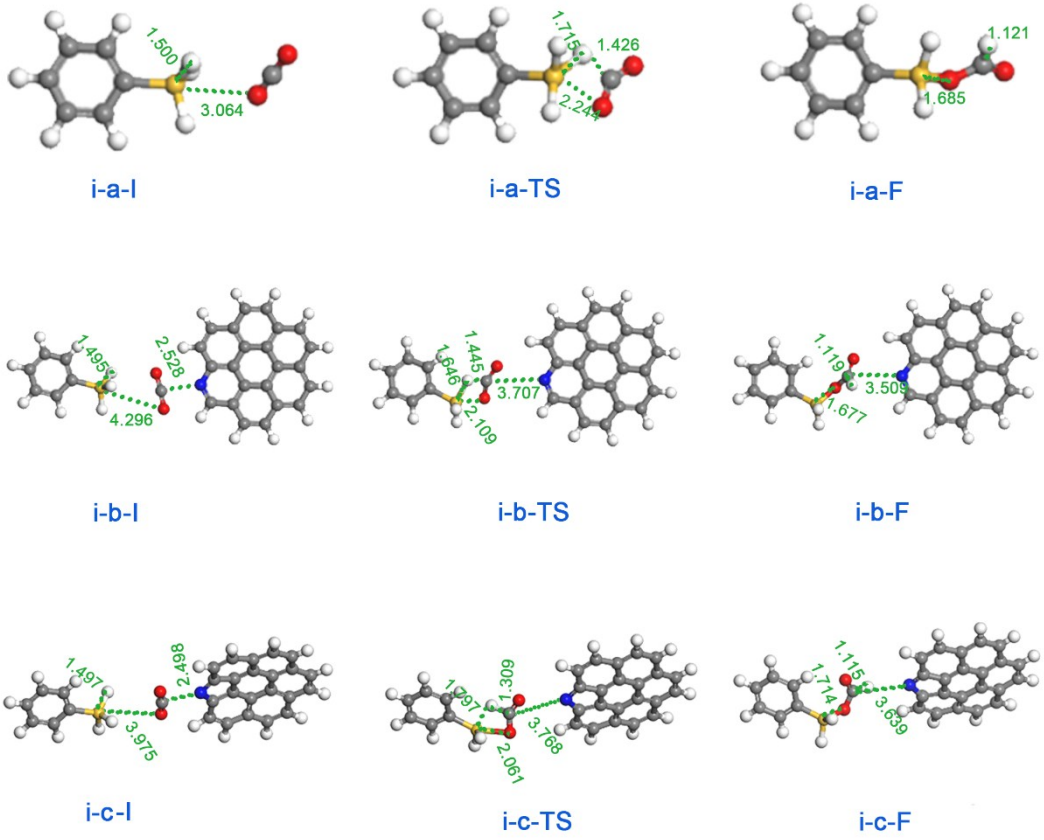

Fig. S13. Optimized initial state (I), transition state (TS) and final state (F) structures involved in step i. Some selected distances are given in Å.

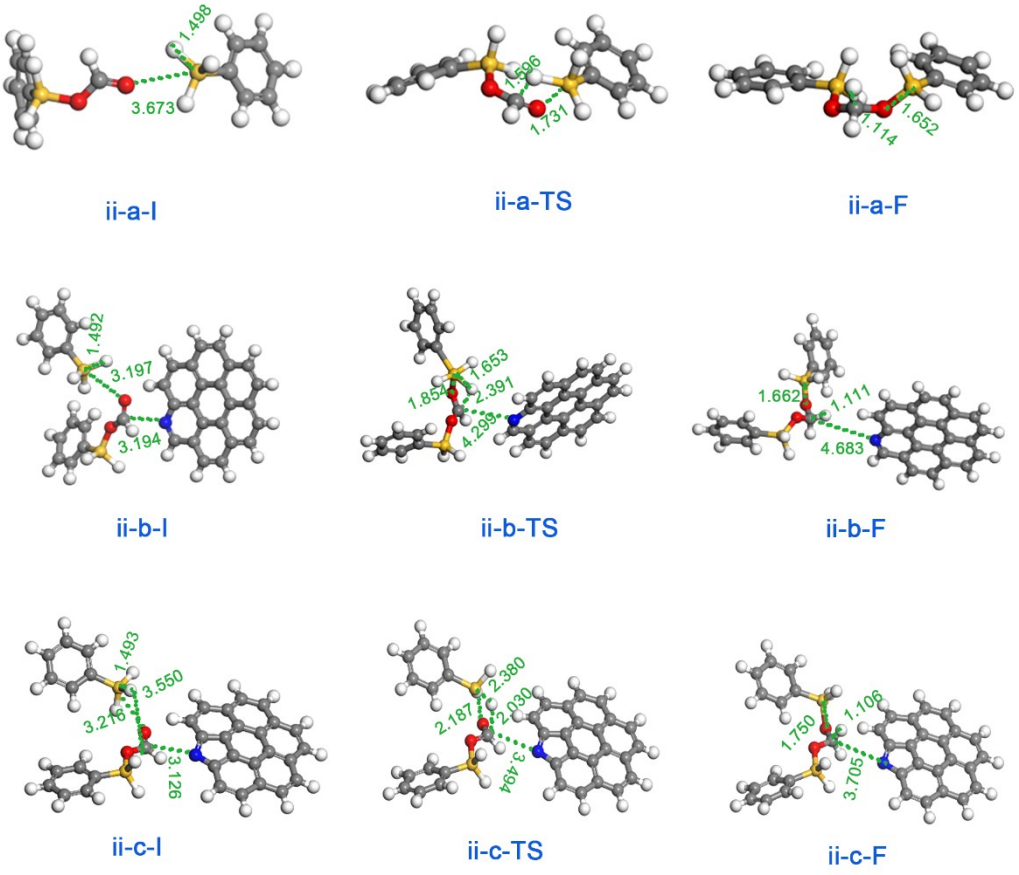

Fig. S14. Optimized initial state (I), transition state (TS) and final state (F) structures involved in step ii. Some selected distances are given in Å.

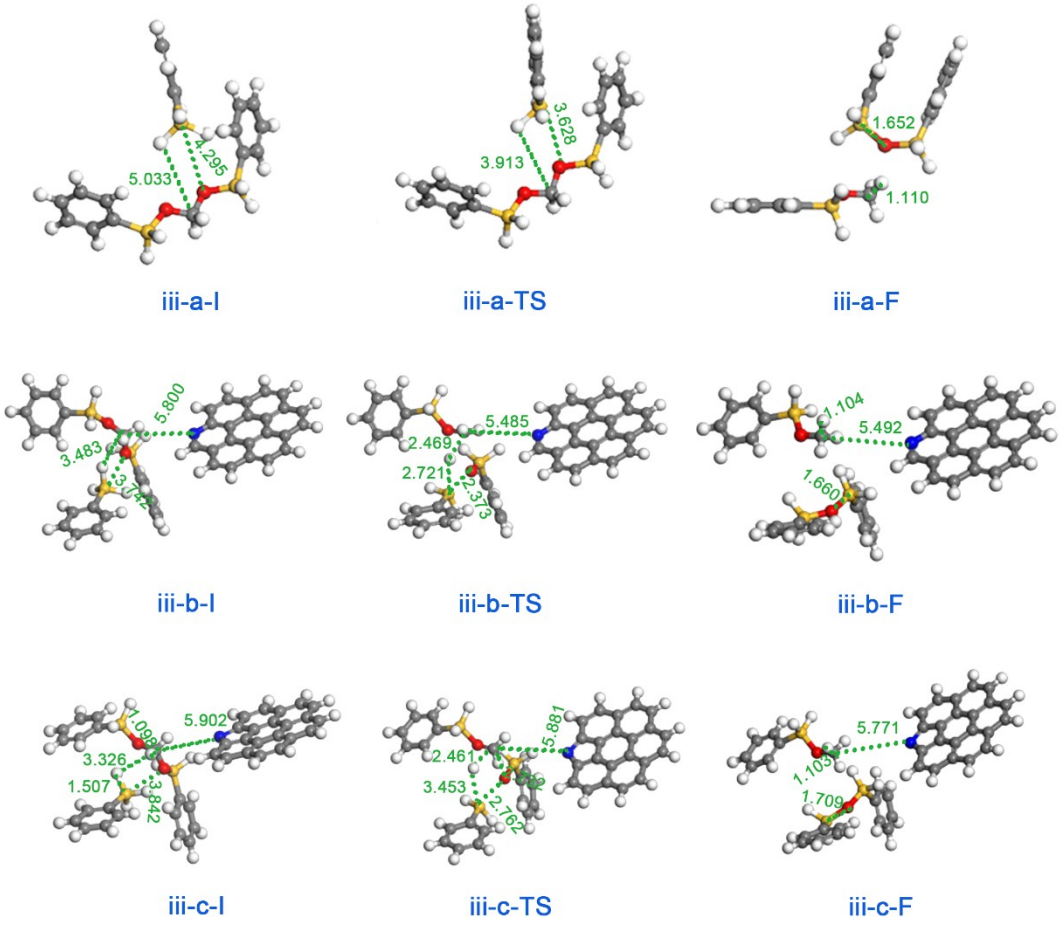

Fig. S15. Optimized initial state (I), transition state (TS) and final state (F) structures involved in step iii. Some selected distances are given in Å.

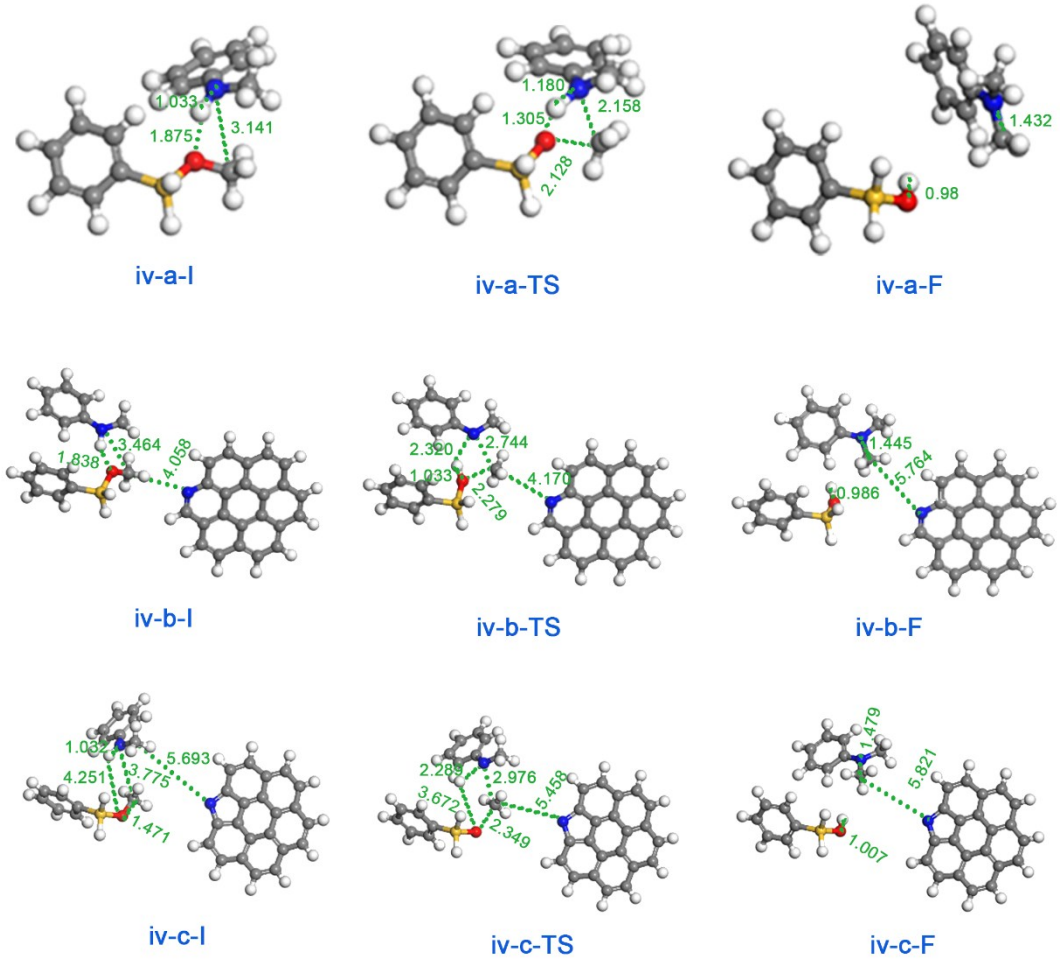

Fig. S16. Optimized initial state (I), transition state (TS) and final state (F) structures involved in step iv. Some selected distances are given in Å.

4. Tables

Table S1. Summary of N 1s XPS results for NPC samples.

Sample	Total N (at%)	Pyrrole-like-N (at%)	Pyridinic N (at%)	Graphitic N (at%)	Pyridine-N-oxide (at%)
$NPC_{(1/2)}$	7.6	0.5	3.6	3.1	0.4
$NPC_{(1/3)}$	7.8	0.5	3.1	3.4	0.8
`$NPC_{(1/5)}$	8.2	0.7	4.0	2.7	0.8
$NPC_{(1/7)}$	8.3	0.5	3.8	3.5	0.5

Table S2. Summary of surface areas and pore volumes for all NPC samples.

Sample	S_{BET}[a]	S_{micro}[b]	S_{meso}[c]	V_{total}[d]	V_{micro}[e]
$NPC_{(1/2)}$	107.6	56.5	51.1	0.20	0.05
$NPC_{(1/3)}$	146.5	84.5	62.0	0.28	0.06
$NPC_{(1/5)}$	216.8	135.8	81.0	0.33	0.10
$NPC_{(1/7)}$	242.8	137.1	105.7	0.46	0.10

Note: [a] Calculated by using the BET model (unit: $m^2\ g^{-1}$); [b] Cumulative micropore surface area with the pore width less than 2 nm using NLDFT model (unit: $m^2\ g^{-1}$); [c] $S_{meso}=S_{BET}-S_{micro}$ (unit: $m^2\ g^{-1}$); [d] V_{total}: total volume (unit : $cm^3\ g^{-1}$), calculated at $P/P_0 = 0.99$; [e] V_{micro}: Micropore volume (unit : $cm^3\ g^{-1}$), calculated from NLDFT.

Table S3. Catalytic performance of $NPC_{(1/5)}$ in different solvents.

Entry	Catalyst	Solvent	P_{CO2} (bar)	T (°C)	t (h)	C (%)	S (%)	
							1b	1c
1	$NPC_{(1/5)}$	CH_3OH	1	75	18	Trace	–	–
2	$NPC_{(1/5)}$	1,4-dioxane	1	75	18	63.1	88.0	12.0
3	$NPC_{(1/5)}$	CH_3CN	1	75	18	80.1	83.9	16.1
4	$NPC_{(1/5)}$	DMSO	1	75	18	67.8	87.0	13.0
5	$NPC_{(1/5)}$	DMF	1	75	18	97.1	90.2	9.8
6	$NPC_{(1/5)}$	THF	1	75	18	56.8	84.4	15.6
7	–	CH_3OH	1	75	18	Trace	–	–
8	–	1,4-dioxane	1	75	18	Trace	–	–
9	–	CH_3CN	1	75	18	2.1	83.0	17.0
10	–	DMSO	1	75	18	37.8	86.2	13.8
11	–	DMF	1	75	18	64.1	78.9	21.1
12	–	THF	1	75	18	Trace	–	–
13	Pyridine	THF	1	75	18	32.6	78.1	21.9
14	Pyrrole	THF	1	75	18	Trace	–	–

Reaction condition: 1a (0.25 mmol), $PhSiH_3$ (0.5 mmol), catalyst (15 mg), solvent (3 mL); Conversion rate (C) and Selectivity (S) were determined by HPLC.

Table S4. The Methylation reaction of N-methylaniline with CO_2 over our proposed NPC catalysts and recently documented homogenous catalysts.

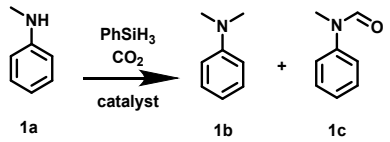

Catalyst	CO_2 (bar)	T (^oC)	Conversion of 1b (%)	Yield of 1b (%)	Selectivity of 1b (%)
DBU[1]	1	100	–	88.0	–
NHC B[2]	1	50	–	84.0	–
GB[3]	1	70	>99.0	91.0	–
DMF[4]	1	90	–	80.0	–
$[RhCl\{C(NCH_2PCy_2)_2C_{10}H_6]$[5]	1	90	98.0	93.0	–
$Mn_2(CO)_{10}$ /L1[6]	1	100	–	87.0	–
$Cu_2(OH)_2CO_3$/DPPB[7]	1	60	93.0	88.0	95.0
$[RuCl_2(dmso)_4$/nBuPAd$_2$[8]	30	100	–	98.0	–
$CsCO_3$[9]	4	80	–	71.0	–
COF-HNU3[10]	1	30	–	96	99
Gibeon meteorite[11]	10	100	–	96	–
This work	1	75	97.1	87.6	90.2

Table S5. Summary of N 1s XPS results for NPC(1/5) before and after reaction.

Sample	Total N (at%)	Pyrrole-like-N (at%)	Pyridinic N (at%)	Graphitic N (at%)	Pyridine-N-oxide (at%)
Before	8.2	0.7	4.0	2.7	0.8
After	8.4	0.8	3.9	3.1	0.6

Reference

1. G. Li, J. Chen, D.-Y. Zhu, Y. Chen and J.-B. Xia, Adv. Synth. Catal., 2018, 360, 2364-2369.
2. S. Das, F. D. Bobbink, G. Laurenczy and P. J. Dyson, Angew. Chem. Int. Ed., 2014, 53, 12876-12879.
3. X. F. Liu, X. Y. Li, C. Qiao, H. C. Fu and L. N. He, Angew. Chem. Int. Ed., 2017, 56, 7425-7429.
4. H. Niu, L. Lu, R. Shi, C. W. Chiang and A. Lei, Chem. Commun., 2017, 53, 1148-1151.
5. R. H. Lam, C. M. A. McQueen, I. Pernik, R. T. McBurney, A. F. Hill and B. A. Messerle, Green Chem., 2019, 21, 538-549.
6. Z. Huang, X. Jiang, S. Zhou, P. Yang, C. X. Du and Y. Li, ChemSusChem, 2019, 12, 3054-3059.
7. X.-D. Li, S.-M. Xia, K.-H. Chen, X.-F. Liu, H.-R. Li and L.-N. He, Green Chem., 2018, 20, 4853-4858.
8. Y. Li, X. Fang, K. Junge and M. Beller, Angew. Chem. Int. Ed., 2013, 52, 9568-9571.
9. C. Fang, C. Lu, M. Liu, Y. Zhu, Y. Fu and B.-L. Lin, ACS Catal, 2016, 6, 7876-7881.
10. J. Qiu, Y. Zhao, Z. Li, H. Wang, Y. Shi, J. Wang, ChemSusChem 2019, 12, 2421-2427.
11. A. Gopakumar, I. Akçok, L. Lombardo, F. Le Formal, A. Magrez, K. Sivula, P. J. Dyson, ChemistrySelect 2018, 3, 10271-10276.

.